JACS
JOURNAL OF THE AMERICAN CHEMICAL SOCIETY

Article

pubs.acs.org/JACS

Covalent Immobilization of a Molecular Catalyst on Cu_2O Photocathodes for CO_2 Reduction

Marcel Schreier, Jingshan Luo, Peng Gao, Thomas Moehl,[†] Matthew T. Mayer,* and Michael Grätzel*

Institut des Sciences et Ingénierie Chimiques, Ecole Polytechnique Fédérale de Lausanne, Station 6, CH-1015 Lausanne, Switzerland

Supporting Information

ABSTRACT: Sunlight-driven CO_2 reduction is a promising way to close the anthropogenic carbon cycle. Integrating light harvester and electrocatalyst functions into a single photoelectrode, which converts solar energy and CO_2 directly into reduced carbon species, is under extensive investigation. The immobilization of rhenium-containing CO_2 reduction catalysts on the surface of a protected Cu_2O-based photocathode allows for the design of a photofunctional unit combining the advantages of molecular catalysts with inorganic photoabsorbers. To achieve large current densities, a nanostructured TiO_2 scaffold, processed at low temperature, was deposited on the surface of protected Cu_2O photocathodes. This led to a 40-fold enhancement of the catalytic photocurrent as compared to planar devices, resulting in the sunlight-driven evolution of CO at large current densities and with high selectivity. Potentiodynamic and spectroelectrochemical measurements point toward a similar mechanism for the catalyst in the bound and unbound form, whereas no significant production of CO was observed from the scaffold in the absence of a molecular catalyst.

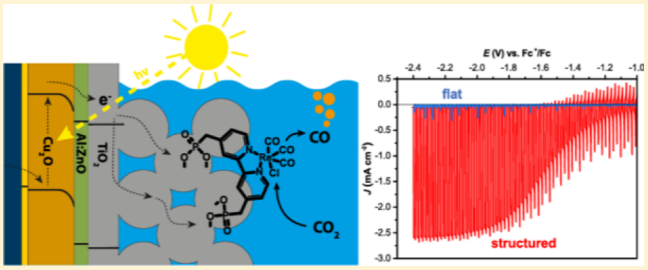

INTRODUCTION

Ever increasing atmospheric concentrations of carbon dioxide (CO_2) are having a profound impact on the world's climate system.[1] The need to control CO_2 levels has led to intense research into alternative energy systems that do not rely on fossil fuels as a source of primary energy. Solar energy is an overwhelmingly abundant resource great enough to fulfill all of the world's energy demands,[2] but due to its intermittent nature, it must be stored to become a truly useful source of energy.[3] Various approaches for the storage of solar power have been investigated, including its direct transformation into chemical energy to yield "solar fuels", which has received substantial interest in recent years.[4,5] The most attractive approach entails using sunlight to reduce CO_2 into carbon-based fuels,[6−8] thereby allowing the use of the existing energy infrastructures while simultaneously closing the anthropogenic carbon cycle.

Achieving direct conversion of sunlight and CO_2 into chemical fuels requires the linking of light-absorbing and catalytic components, accomplished in nature by the process of photosynthesis. A promising artificial system for the production of solar fuels at higher efficiency than the natural counterpart is the photoelectrochemical cell,[9] a device in which semiconductors, functionalized with catalysts, are illuminated while immersed in an electrolyte containing the reactants. Photogenerated charges in the semiconductor are separated and directed to the respective catalysts, where they subsequently drive the fuel-generating reactions. This approach has been extended to tandem structures, achieving unassisted water splitting and CO_2 reduction.[10−16]

The development of efficient and selective catalysts is crucial to the success of catalytic fuel-forming reactions. Molecular catalysts for hydrogen evolution[17,18] and carbon dioxide reduction[19] have attracted significant attention due to their well-controlled properties and tunable nature, making them an interesting subject of study. Significant progress has been made with respect to stability[20] and activity toward the desired reactions.[21]

An attractive approach to driving molecular catalysts using the power of sunlight is to incorporate the catalysts into photoelectrochemical systems. Such an application can be achieved in either homogeneous or heterogeneous approaches, whereas the former employs the catalysts as a dissolved species in the electrolyte.[7,22,23] This, however, requires large amounts of catalyst, most of which is not actively participating in the reaction and, in addition, causes parasitic light absorption, thereby limiting the photocurrent density observed from these systems.[7,24] Furthermore, many molecular catalysts rely on precious-metal centers, thus providing incentive for minimizing the amount of required catalyst as much as possible. Both of these challenges can be addressed by binding the molecular catalyst directly to the surface of the photoelectrode, which comes down to heterogenizing a homogeneous catalyst. Thereby, the use of catalyst is reduced to an amount that is actively participating in the reaction, and some recent works have demonstrated the ability of this approach to significantly

Received: November 20, 2015
Published: January 23, 2016

DOI: 10.1021/jacs.5b12157
J. Am. Chem. Soc. 2016, 138, 1938−1946

improve catalytic yield in electrocatalytic and photocatalytic systems.[25−28]

Recently, the use of metal oxides, particularly TiO_2, toward the protection of otherwise unstable photoelectrode materials, such as Cu_2O, has drawn much attention in the solar fuels research community.[8,29−31] These metal oxide overlayers constitute an ideal substrate for the covalent binding of molecules by the means of molecular linking groups such as carboxylates and phosphonates,[26,32−34] approaches that have been crucial toward the realization of efficient dye-sensitized solar cells.[35] However, despite the attractive prospect of decreasing catalyst loading while retaining efficiency, few examples of molecular catalysts linked to surfaces of photoelectrodes have been shown.[36−38] In the case of CO_2 reduction, all reports on immobilized catalysts have so far focused on dye−catalyst complexes[39,40] and polymer films.[12−14,41−43]

Here, we demonstrate for the first time the production of carbon monoxide (CO) as a solar fuel by the covalent attachment of molecular CO_2 reduction catalysts to the surface of TiO_2-protected Cu_2O photocathodes by the means of phosphonate linkers (Figure 1). CO is an attractive target for solar fuel synthesis due to its application in the Fischer−Tropsch and gas-to-methanol processes, which allow its transformation into virtually any carbon-based fuel, the cost of which is largely driven by the preparation of syngas.[44] Importantly, we show that the presence of a low-temperature-processed mesoporous scaffold on the surface of the photoelectrode is a crucial requirement to achieve efficient CO_2 catalysis, demonstrating an innovative and important application of these scaffolds that originally enabled the breakthrough of dye-sensitized solar cells.[35]

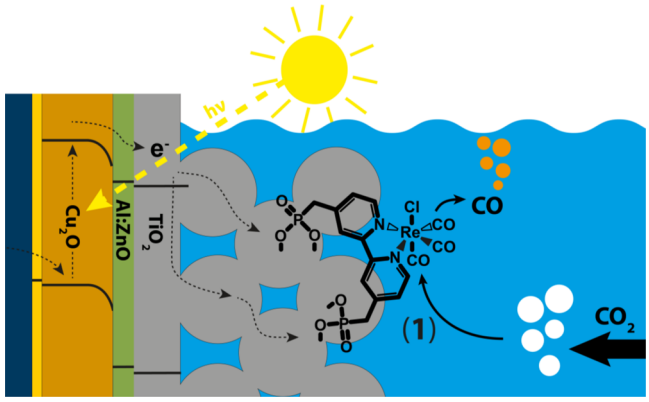

Figure 1. Schematic (not to scale) of protected Cu_2O photoelectrode with covalently bound Re(bipy) CO_2 reduction catalyst **1**.

RESULTS AND DISCUSSION

Virtues of the Mesoporous Scaffold. Complexes based on Re, particularly $Re(bpy)(CO)_3Cl$ first introduced by Lehn and co-workers, have shown excellent performance as well as robustness when used as homogeneous electrocatalysts for the selective conversion of CO_2 to CO in acetonitrile.[19,21,45,46] At the same time, TiO_2-protected Cu_2O photoelectrodes hold the record performance as low-cost p-type light harvesters for water splitting.[29] To enable covalent binding to the TiO_2 surface protecting the Cu_2O photocathode, the bipyridyl ligand of the original Lehn complex was modified with phosphonate linking groups to form catalyst **1** [Figure 1 and Figure S1 of the Supporting Information (SI)]. A methylene bridge was incorporated between the phosphonate and bipyridyl moiety to minimize modification of the electronic structure of the catalyst, a negative consequence of the ligand modification as has been described elsewhere.[45]

Cu_2O photocathodes were prepared by electrodeposition followed by atomic layer deposition of 20 nm of Al-doped ZnO (AZO) and 100 nm of TiO_2, as previously described.[29] The TiO_2 surface was subsequently functionalized with catalyst **1** by soaking the device in a 1 mM solution of catalyst in MeCN for 24 h, followed by copious rinsing with neat MeCN. However, subsequent photoelectrochemical testing did not show substantial photocurrents, pointing toward the absence of catalytic activity. The maximum photocurrent densities under CO_2 were found to be merely 65 μA cm^{-2}, which indicated a negligible rate of catalytic charge transfer under these conditions (Figure S2, SI).[7,29] In addition, measurements with varying light intensities showed a nonlinear photocurrent response, indicating an impeded charge extraction that leads to major charge recombination within the photoelectrode. Therefore, the simple functionalization of a standard Cu_2O photocathode with catalyst **1** was found to be inadequate for achieving significant rates of light-driven CO_2 reduction.

We hypothesized that the catalyst loading on this flat TiO_2 surface was too low to achieve significant currents, introducing a bottleneck to the flux of photogenerated charge from the photocathode. This was further confirmed by FTIR, showing no signal relative to any bound catalyst. In their early stages of development, dye-sensitized solar cells suffered from analogous limitations, where the light absorption of a planar device was too low to achieve high efficiency, a problem eventually overcome by loading the dyes onto thick, transparent films of mesoporous TiO_2.[35] We theorized that a similar approach might find success here, wherein enhancing the roughness factor and catalyst loading could enable better compatibility with the photogenerated electron flux from the photocathode; therefore, we sought to deposit porous films atop the photocathode surface.

These mesoporous TiO_2 films are traditionally processed at 500 °C in air, a treatment necessary to oxidize the binder material and to sinter the TiO_2 particles.[47] Unfortunately, this method is not compatible with the photocathode employed here, since the p−n junction between Cu_2O and AZO has been found to deactivate upon heating beyond 250 °C, thereby precluding any high-temperature treatment for protected Cu_2O photocathodes.[48] However, the curing of TiO_2 films under ultraviolet (UV) light has shown promising results as an alternative to high-temperature processing.[49,50] Inspired by these works, mesoporous films of 4.5 to 5 μm thickness with 18 nm TiO_2 particles were deposited onto fluorine-doped tin oxide (FTO) substrates and treated by UV light at room temperature for 48 h followed by $TiCl_4$ processing at 70 °C. The $TiCl_4$ treatment was found to be the key to achieve films that were stable under the testing conditions.

Catalyst Immobilization on Low-Temperature Mesoporous TiO_2 Films. The successful UV curing of TiO_2 films was confirmed by FTIR measurements, showing the disappearance of modes associated with ethyl cellulose for both thermally cured[47] and UV-cured films (Figure 2a). From ac-impedance measurements, it was found that films prepared at low temperature showed an additional resistor−capacitor element that could be attributed to a contact resistance between individual particles. Interestingly, this element almost completely disappeared at more negative potentials as shown in

DOI: 10.1021/jacs.5b12157
J. Am. Chem. Soc. 2016, 138, 1938−1946

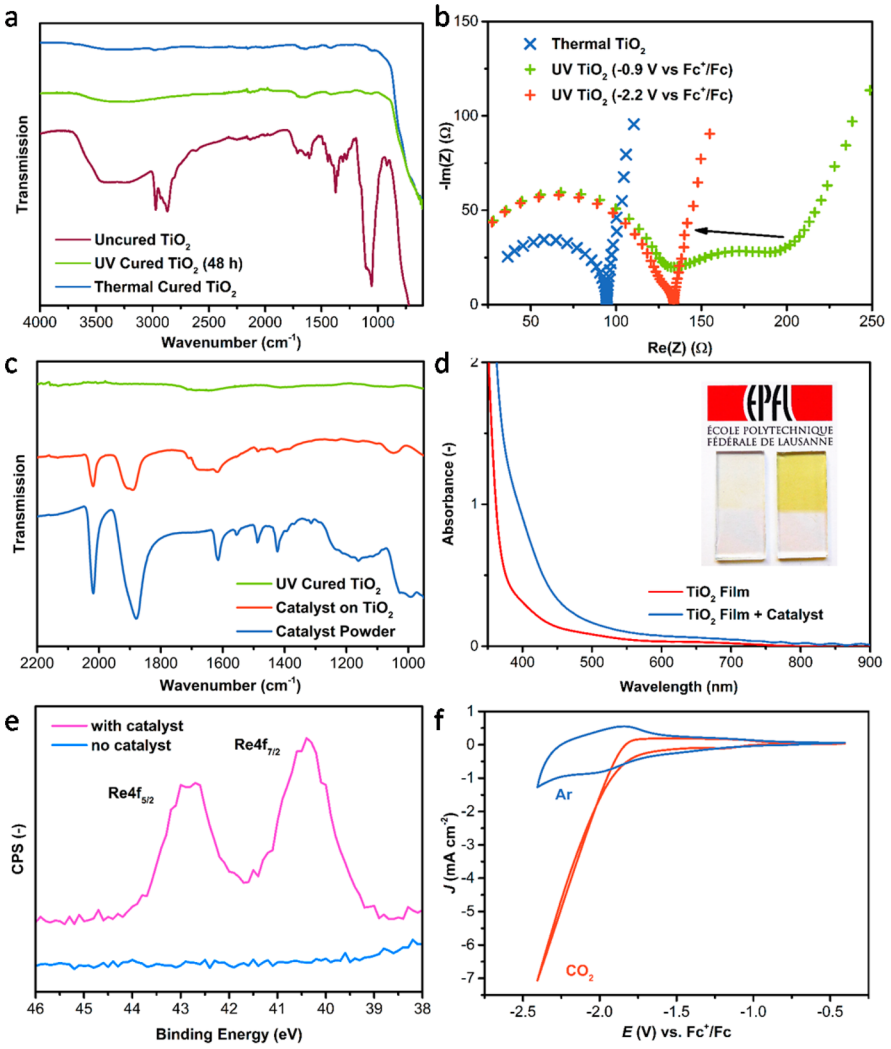

Figure 2. (a) FTIR-ATR measurement of TiO_2 films before curing and after thermal and UV curing. Ethyl cellulose is efficiently eliminated upon UV curing, yielding films that are essentially indistinguishable from those produced by thermal processing. (b) EIS spectra of thermally cured and UV-cured films. The additional charge transfer resistance that is observed for UV-cured films disappears at more negative potentials. (c) FTIR-ATR measurements of films before and after binding of catalyst **1**, compared to the catalyst powder spectrum, confirming catalyst binding to the film. (d) Optical absorption spectra of TiO_2 films with and without bound catalyst. The inset shows a photo of a TiO_2 film with and without bound catalyst, as an illustration of the catalyst color. (e) XPS detail spectrum of the Re 4f peak, confirming the presence of Re catalyst on the TiO_2 film surface compared to a UV-cured TiO_2 film without catalyst. (f) Cyclic voltammetry of catalyst **1** bound to UV-cured TiO_2 on FTO. The catalytic onset can be clearly distinguished in the presence of CO_2.

Figure 2b, and the films thus behave similar to thermally cured films under these conditions.

After heating the samples to 150 °C under vacuum to remove water from the scaffold, catalyst **1** was applied onto the surface of mesoporous TiO_2 by soaking the substrate in a 1 mM solution of **1** for 24 h. The samples were then copiously rinsed with MeCN to ensure removal of any unbound species. To verify for the presence of bound catalysts, FTIR-ATR measurements were carried out on the sample surface. As shown in Figure 2c, strong peaks corresponding to the carbonyl vibrations on the Re complex could be observed at 1911 and 2035 cm^{-1}, which are not present on a bare TiO_2 sample before the treatment with catalyst. These peaks are blue-shifted in the bound form as compared to their powder spectrum (1868 and 2012 cm^{-1}), suggesting a decreased electron density on the Re center upon binding to TiO_2. The bound catalyst introduced a slight yellow coloration of the TiO_2 films, as can be seen from the photographs and UV−vis transmission spectra in Figure 2d.

The presence of grafted catalyst was further confirmed by X-ray photoelectron spectroscopy (XPS) measurements on the photocathodes, which show the appearance of a clearly visible signal for Re (Figure 2e) at 40.4 and 42.7 eV, in agreement with previously reported values.[51] Additionally, nitrogen and phosphorus as well as oxygen due to the complex could be confirmed (Figure S3, SI). The amount of catalyst present on the scaffold was determined by ICP-OES of rhenium after complete dissolution in acid and found to be ~85 nmol cm^{-2}.

To prove that binding was mediated by the phosphonate group and indeed was covalent, the catalyst-binding procedure was repeated using a complex without binding group (species **2**, Figure S1, SI).[7,45] After rinsing, no FTIR signal from bound molecules could be observed in this case (Figure S4, SI), thereby establishing that the phosphonate groups were crucial for achieving catalyst immobilization on the scaffold.

Electrochemical Characterization of Immobilized Catalyst. To examine the electrochemical behavior of the

DOI: 10.1021/jacs.5b12157
J. Am. Chem. Soc. 2016, 138, 1938−1946

unbound catalyst itself, cyclic voltammetry scans were carried out on a MeCN solution of catalyst **1** using a glassy carbon electrode (Figure S5, SI). After a first reduction at −1.62 V vs Fc^+/Fc, two minor reduction peaks could be observed at −1.77 and −1.88 V. Under CO_2, the second peak leads into a catalytic wave, confirming the activity of the complex toward reducing CO_2. Furthermore, as a positive side effect of the bipyridine modification, its catalytic onset is shifted 195 mV positive compared to $Re(bpy)(CO)_3Cl$, which was introduced by Lehn and co-workers (Figure S5, SI).[46] Cyclic voltammetry measurements of catalyst **1** bound to UV-cured TiO_2 films show a strong activity toward the electroreduction of CO_2 (Figure 2f), exhibiting current densities exceeding 7 mA cm^{-2} at −2.4 V vs Fc^+/Fc in the presence of CO_2. The onset of current is observed at approximately −1.7 V vs Fc^+/Fc in only one reduction peak, which is interesting since commonly Re(bpy) catalysts are known to be activated through a two-step reduction process in systems where homogeneously dissolved catalyst is driven by an inert electrode.[45,52]

To investigate the catalytic activation in the present system, UV−vis spectroelectrochemical experiments were carried out. The system under study offers a powerful tool for combining electrochemical and spectroscopic study. The scaffold roughness enables the presence of a high density of grafted species, while the semitransparency of the TiO_2 scaffold allows the use of transmittance-based measurements. From the analysis of potential-dependent light absorption (Figure S6, SI), we observed a catalyst transition characterized by two absorption peaks at 507 and 578 nm appearing at −1.9 V vs Fc^+/Fc when polarized in the absence of CO_2, a potential coinciding with the catalytic onset under CO_2 as shown in Figure 2f. We attribute the spectral change to the formation of a stable anion of catalyst **1**.[52] Furthermore, this absorption was only observed in the presence of Ar, but not under CO_2, indicating that the observed species is being rapidly turned over in the presence of carbon dioxide and suggesting that it corresponds to the catalytically active species. In addition, the onset of catalytic current from the unbound catalyst at the glassy carbon electrode (Figure S5, SI) was observed at the same potential. These data and the spectroelectrochemical observation of a catalytically active intermediate at the potential of the catalytic reduction event at the glassy carbon electrode lead us to the conclusion that the catalytic mechanism remains unchanged by binding the catalyst to the TiO_2 scaffold.

CO_2 Reduction Photoelectrocatalysis. Having established UV-cured TiO_2 as a viable substrate for active grafted catalysts, we applied this low-temperature process to deposit the mesoporous scaffold onto $Cu_2O/AZO/TiO_2$ photocathodes. The different layers of the device can be clearly distinguished from the electron micrographs shown in Figure 3. Layer thicknesses are indicated in the figure caption. The layers fulfill the following functions: Cu_2O serves as photoabsorber and forms a p−n junction with AZO, whereas the atomic layer deposited (ALD) TiO_2 layer serves as a protective layer to avoid photocorrosion of Cu_2O, and mesoporous TiO_2 serves as a scaffold to support the molecular catalyst.[29] Due to its nature as a buried p−n junction device,[53] the transfer of electrons to the catalyst is dictated by the offset of the conduction band of TiO_2 and the catalyst redox potential. The flatband potential of mesoporous TiO_2 in acetonitrile is known to be in the range of −2.4 V vs Fc^+/Fc,[54] whereas the onset of catalytic activity of catalyst **1** at the glassy carbon electrode is observed at −1.9 V vs Fc^+/Fc. Thus, a significant driving force

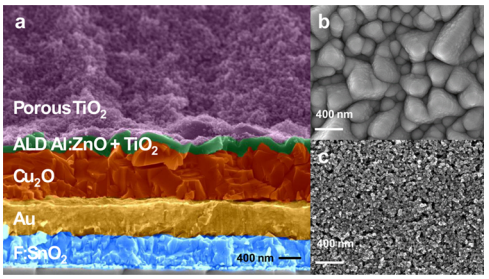

Figure 3. (a) SEM cross section of the modified photoelectrode. Layers have been colored for better readability. The device has the following structure: FTO (580 nm), gold (550 nm), Cu_2O (500 nm−1 μm), ALD Al:ZnO (20 nm), ALD TiO_2 (100 nm), mesoporous TiO_2 (4.5−5 μm, full scale shown in Figure S7, SI). (b) Top-down view of the unmodified photoelectrode surface (corresponding to the green layer in part a) exhibiting low roughness and (c) the surface after adding the mesoporous TiO_2 network, which leads to a highly porous structure, exhibiting a large surface area.

can be expected to exist for electron transfer to take place. A linear sweep voltammogram of the mesoporous-TiO_2-modified photoelectrode loaded with catalyst **1** is shown in Figure 4a. Under CO_2, substantial photocurrents exceeding 2.5 mA cm^{-2} were observed. Importantly, the presence of a mesoporous scaffold led to a 40-fold increase in current compared to that of flat photocathodes. In comparison to the catalyst activity on a dark electrode, i.e., a mesoporous TiO_2 film deposited directly on FTO (Figure 2f), the catalytic current begins at potentials about 600 mV more positive on the photoelectrode, defining the photovoltage produced by the electrode. Both the photocurrent density and photovoltage achieved here represent an improvement over our previous work wherein a protected Cu_2O photocathode was immersed in a solution of dissolved catalyst,[7] and the enhancement in photocurrent can be largely attributed to decreased parasitic light absorption by the catalyst when it is selectively grafted onto the electrode surface. A linear dependence on incident light intensity was observed for this system (Figure S8, SI), showing that the catalyst is now capable of supporting the flux of photogenerated electrons from the photocathode, enabled by loading onto the high area surface of the mesoporous TiO_2 scaffold.

Our previous observations when using a photocathode to drive a homogeneous catalyst in solution led to the hypothesis that consecutive catalyst reductions were hindered by electrostatic repulsion between the polarized semiconductor electrode and charged catalyst intermediates inhibiting subsequent CO_2 reduction.[7] In that study, the inhibition could be surmounted by addition of a protic additive to solution. In this report, efficient catalyst turnover was accomplished without the need for protic additives, demonstrating how covalently linking the catalyst to the electrode surface is a useful approach toward enabling sequential charge transfer between the semiconductor electrode and CO_2 reduction catalyst, in addition to greatly decreasing the required catalyst amount and minimizing its parasitic absorption.

Potentiostatic testing at −1.9 V vs Fc^+/Fc under chopped-light illumination showed sustained catalytic activity toward the reduction of CO_2 (Figure 4b), during which a gradual decrease in photocurrent could be observed, as will be discussed below.

In order to verify the catalytic activity toward CO_2 conversion, the evolved gases were quantified by gas chromatography during constant polarization of UV-cured

DOI: 10.1021/jacs.5b12157
J. Am. Chem. Soc. 2016, 138, 1938−1946

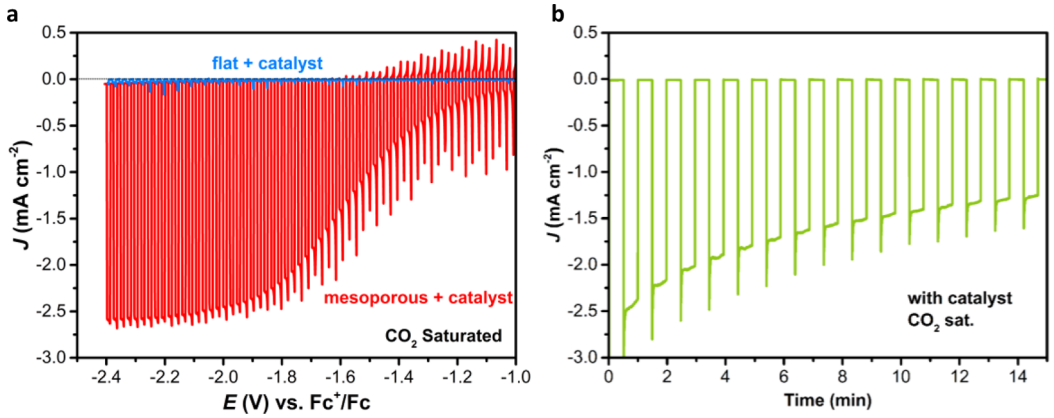

Figure 4. (a) Photoelectrochemical performance under chopped, simulated sunlight of Cu_2O photocathodes with (red) and without (blue) a mesoporous TiO_2 layer on the surface, tested under CO_2 with molecular Re catalyst covalently bound to the surface. Linear sweep at 10 mV s^{-1}. (b) Chopped-light polarization test under CO_2 at −1.9 V vs Fc^+/Fc of a mesoporous TiO_2 layer modified Cu_2O photocathode with catalyst.

TiO_2-supported catalyst on FTO. It was found that the sample reached Faradaic yields for CO between 80 and 95%, whereas in the absence of catalyst, negligible CO was observed (Figure 5). Furthermore, when polarized under inert helium saturation, no production of gas-phase species was observed (Figure S9, SI). Taken together with the high turnover numbers observed, as estimated below, these experiments indicate that the observed carbon monoxide originates from a catalytic reaction of CO_2, rather than from decomposition of the catalyst, and that the molecular catalyst is indeed required for turnover of CO_2 to take place.

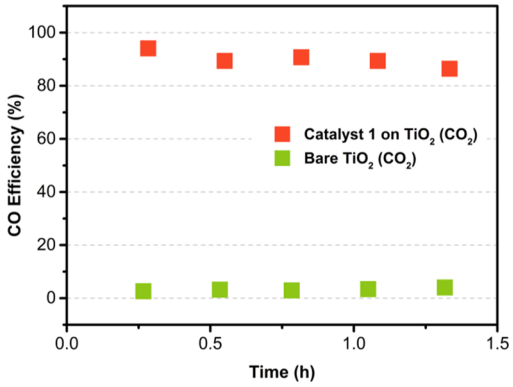

Figure 5. Quantification of the Faradaic efficiency of carbon monoxide production by catalyst-modified TiO_2 films polarized at −2.05 V vs Fc^+/Fc and from a bare TiO_2 film at −2.20 V vs Fc^+/Fc under CO_2 saturation. The presence of catalyst is necessary for CO_2 to be turned over.

Loss of Catalytic Activity. During potentiostatic testing of the photoelectrode under chopped light, a gradual decrease in photocurrent (Figure 4b) and in Faradaic efficiency for CO (Figure 5) was observed over time. To shed light on these processes, a series of techniques were used to determine the changes to the electrodes resulting from extended operation. After 2 h of polarization at −1.9 V vs Fc^+/Fc under chopped light of a catalyst-coated photoelectrode followed by rinsing in neat MeCN, surface analysis by XPS confirmed the persistence of the elements attributable to the immobilized catalyst (Re, N, and P), albeit at a slightly lower intensity (Figure S3, SI). The peaks associated with Re did not experience a significant shift, indicating no change in oxidation state. At the same time, FTIR-ATR spectra showed the persistence of the C−O stretches related to the bound catalyst, similarly at a slightly reduced intensity (Figure S10, SI). From the observation of a decreased signal intensity, one may assume that a part of the

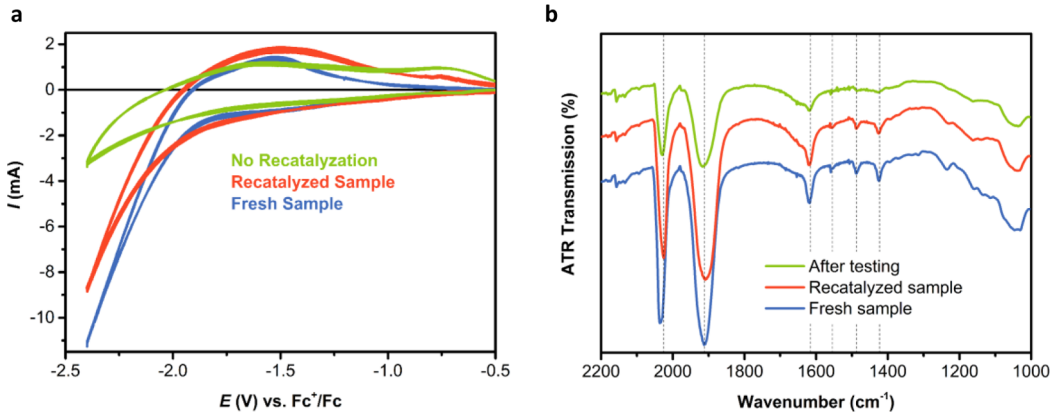

Figure 6. (a) CV curves recorded from a thermally treated TiO_2 sample at different stages of testing. The re-exposure of a deactivated sample to fresh catalyst (red trace) led to a performance comparable to that of the fresh sample (blue trace). In contrast, the performance of a sample tested for 3 h without recatalyzation (green trace) is significantly lower than that of a fresh sample. (b) At each stage of the experiment ATR-FTIR measurements were carried out. The C−O stretches associated with the catalyst are observed at each stage.

DOI: 10.1021/jacs.5b12157
J. Am. Chem. Soc. 2016, 138, 1938−1946

catalyst is desorbing, which is the most straightforward explanation for the decrease in photocurrent. However, further experiments gave evidence that other processes, such as the structural change of the catalysts, are likely to play a role. Our previous report rules out the instability of the Cu_2O photoabsorber underlayer,[7] but the issue remains for catalyst and TiO_2 mesoporous scaffold. To eliminate the contribution from the scaffold, additional experiments were conducted using thermally cured mesoporous TiO_2 films on FTO, where a similar degradation was observed, suggesting that the scaffold does not play a role in the deactivation process. Furthermore, it was found that immersing a completely deactivated sample in a 1 mM solution of catalyst for 24 h led to almost complete recovery of the catalytic activity (Figure 6a). In contrast, when a deactivated sample was rinsed, dried, and subsequently tested in fresh electrolyte, no regain of activity was observed. Despite the loss of catalytic activity, the presence of catalyst was consistently observed by FTIR spectroscopy in between the measurements (Figure 6b). It is notable that even after 3 h of polarization at −2.2 V vs Fc^+/Fc, strong signals from the catalyst C−O stretches were visible. Despite being weaker than in the case of a fresh sample, the observation of these signals indicates that loss of catalyst is not the only process leading to the observed decrease in current. Support for this conclusion comes from ICP-OES analysis, which even after 3 h of continuous polarization still detects between 60 and 70% of the initial rhenium on the substrates (Table S1, SI). Structural change of the catalyst molecules themselves is therefore likely to play a significant role as well, as can be seen from the distinct color change of samples after deactivation (Figure S11, SI). Previously, the formation of a formato−rhenium complex was suggested as being at the origin of the loss of catalytic activity,[55] but in our case no evidence for this effect can be obtained from FTIR, where no significant shift of the carbonyl stretches is observed. In contrast, we find that the vibrations in the region from 1400 to 1600 cm^{-1}, related to the bipyridine group, are bleached after testing, suggesting that a structural change of the bipyridine may lead to catalyst deactivation. This effect is likely intensified by the fact that only a very small amount of catalyst is present in the system, which cannot be replenished by diffusion of pristine catalyst from a bulk solution, as is the case in a homogeneous electrocatalytic system. As an example, from integrating the current toward CO during a 1.5 h test at −2.05 V vs Fc^+/Fc (Figure 5), the catalyst molecules exceed 70 turnovers, which is larger than what was achieved in previous reports under similar conditions.[26,27,51,55,56]

Advantages and Challenges. The catalyst-binding strategy developed here successfully enabled CO_2 reduction to CO while orders of magnitude smaller quantities of expensive catalyst were used as compared to systems of homogeneous catalyst solutions and parasitic absorption due to the catalyst was minimized. Since the covalent linking strategy uses a small amount of catalyst with a high proportion of catalytic participation, in contrast to homogeneous systems, where only a miniscule fraction of catalyst is interacting with the electrode at a given moment, each grafted catalyst molecule experiences a significantly higher number of turnovers. Therefore, it is subject to the acceleration of any degradation pathways, as opposed to cases where abundant fresh catalyst molecules are present in solution. We consider this an advantage of heterogenized homogeneous catalyst systems, since they can provide a more direct picture of catalyst change than is possible in homogeneous systems.

While detailed study of the deactivation is a goal of ongoing work, we have examined the system by multiple techniques before, during, and after operation. The hybrid heterogeneous system demonstrated here should warrant further analysis by in situ techniques (optical spectroscopy, transient absorption spectroscopy) to elucidate the mechanisms, kinetics, and deactivation pathways of molecular catalysts with the added benefit of electrochemical control. Binding the catalyst to an electroactive surface enables biasing all catalyst molecules at the same potential, reduces the influence of diffusion processes, and facilitates the multiple electron transfers necessary for a multistep reaction like CO_2 reduction. For instance, it has been reported that surface immobilization of catalyst can lead to increased lifetimes of catalyst intermediates.[26] This strategy of using immobilized catalysts on a nanostructured scaffold may prove attractive for diverse electrochemical and photoelectrochemical applications, including but not limited to water splitting, CO_2 reduction, and bioelectrochemistry.[57−59]

Although there are reports of immobilized catalysts for heterogeneous photocatalytic CO_2 reduction on particles in solution,[26−28,32−34] relatively few studies exist where catalysts are grafted onto an electrode surface,[41] and there are even fewer that report electrochemical characterization. Among these, to the best of our knowledge, this is the first report of examining the potential and the photoelectrochemistry of phosphonate-mediated covalently bound catalysts for CO_2 reduction. While the performance observed with this system is astonishing and even exceeds the performance recently reported with silicon nanowires,[43] numerous further improvements can be envisioned. Increasing the robustness of the catalyst as well as the binding strategy will improve the stability of the system. Furthermore, the replacement of rhenium with an earth-abundant metal core will lead to a system that is free of precious metals, thereby decreasing the system cost. This will enable another step toward the realization of scalable solar fuels devices, which will be key to achieving an energy system based on renewable resources.

Finally, while the study conducted here examined a photocathode in three-electrode configuration, where the oxidation of the electrolyte serves as the source of electrons, a complete solar-to-fuel conversion process requires a balanced and sustainable counter electrode oxidation process, such as oxygen evolution from water, to supply electrons for the CO_2 reduction reaction.[8,14]

■ CONCLUSION

We demonstrated the light-assisted reduction of carbon dioxide by the use of a covalently bound molecular catalyst on mesoporous-TiO_2-modified Cu_2O photocathodes. The observed photocurrents represent a significant improvement over what has previously been demonstrated with molecular catalysts homogeneously dissolved in the electrolyte solution. Furthermore, in addition to being based on a low-cost photoelectrode, the observed photocurrents are comparable to or better than previous reports of immobilized catalysts on photoelectrodes both toward CO_2 reduction and water splitting. These improvements can largely be attributed to the use of a nanostructured photoelectrode surface, which we have shown to be necessary to achieve large photocurrents with covalently bound catalysts. This work represents the first demonstration of the use of phosphonate linking groups to immobilize a molecular fuel generating electrocatalyst on the surface of a photoelectrode and opens the path toward further

DOI: 10.1021/jacs.5b12157
J. Am. Chem. Soc. 2016, 138, 1938−1946

research into improving the system stability and efficiency, as well as more detailed investigation of the mechanistic details of molecular electrocatalysts.

EXPERIMENTAL SECTION

Synthesis of Catalyst (1). The anchoring bipyridine synthesized for this study has a CH_2 spacer between the PO_3H_2 group and the bipyridine core. A direct link between the catalyst and the semiconductor is not a strict requirement for high electron injection efficiency, and the isolated anchoring group has little influence in the electronic structure of the catalyst itself. Therefore, Re(I) complexes derived from bipyridine **4** were synthesized. Utilization of a spacer group between the phosphonic acid and the bipyridine ligand can also provide a chance to synthesize catalyst **1** with the redox center positioned a considerable distance away from the semiconductor surface.

4,4′-Bis(hydroxymethyl)-2,2′-bipyridine (2). Sodium borohydride (8.2 g) was added in one portion to a suspension of 4,4′-bis(methyl carboxylate)-2,2′-bipyridine (3.0 g, 10.0 mmol) in 200 mL of absolute ethanol. The mixture was refluxed for 3 h and cooled to room temperature, and then 200 mL of an ammonium chloride saturated water solution was added to decompose the excess borohydride. The ethanol was removed under vacuum and the precipitated solid dissolved in a minimal amount of water. The resulting solution was extracted with ethyl acetate (5 × 200 mL) and dried over sodium sulfate, and the solvent was removed under vacuum. The desired solid was obtained in 79% yield and was used without further purification.

^{1}H NMR (400 MHz, CD_3OD, δ): 4.75 (4H, s, CH_2), 7.43 (2H, d, J = 5.5 Hz, aryl H on C5 and C5′), 8.25 (2H, s, aryl H on C3 and C3′), 9.00 (2H, d, J = 5.5 Hz, aryl H on C6 and C6′).

4,4′-Bis(bromomethyl)-2,2′-bipyridine (3). The bipyridine **2** (1.06 g, 4.9 mmol) was dissolved in a mixture of 48% HBr (30 mL) and concentrated sulfuric acid (10 mL). The resulting solution was refluxed (135 °C) for 6 h and then allowed to cool to room temperature, and 40 mL of water was added. The pH was adjusted to neutral with NaOH solution and the resulting precipitate filtered, washed with water (pH 7), and air-dried. The product was dissolved in chloroform (40 mL) and filtered. The solution was dried over magnesium sulfate and evaporated to dryness, yielding 1.42 g of **3** (85% yield) as a white powder.

^{1}H NMR (400 MHz, $CDCl_3$, δ): 4.50 (4H, s, CH_2), 7.38 (2H, d, J = 5 Hz, aryl H on C5 and C5′), 8.45 (2H, s, aryl H on C3 and C3′), 8.68 (2H, d, J = 5 Hz, aryl H on C6 and C6′).

4,4′-Bis(diethylmethylphosphonate)-2,2′-bipyridine (4). A chloroform (8 mL) solution of **3** (1.1 g, 3.2 mmol) and 12 mL of triethyl phosphite was refluxed (156 °C) for 3 h under nitrogen. The excess phosphite was removed under high vacuum, and then the crude product was purified by column chromatography on silica gel (eluent ethyl acetate/methanol 80/20), yielding 1.17 g (80%) of **4**.

^{1}H NMR (300 MHz, $CDCl_3$, δ): 1.29 (12H, t, J = 7 Hz, CH_3), 3.23 (4H, d, J = 22 Hz, CH_2P), 4.09 (8H, apparent quintet, J = 7 Hz, OCH_2), 7.35–7.38 (2H, m, aryl H on C5 and C5′), 8.34–8.37 (2H, m, aryl H on C3 and C3′), 8.62 (2H, d, J = 5 Hz, aryl H on C6 and C6′). ^{31}P NMR (81 MHz, $CDCl_3$, δ): 25.37.

[Re(4,4′-diethylmethylphosphonate-2,2′-bipyridine)(CO)$_3$Cl] (5). $Re(CO)_5Cl$ (0.5 g, 1.38 mmol) was dissolved in 50 mL of hot toluene. An equimolar amount of 4,4′-bis(diethylmethylphosphonate)-2,2′-bipyridine (0.630 g, 1.38 mmol) was added to the hot solution, and the reaction mixture was stirred under reflux for 1 h. Once the solution reached reflux, the mixture began to change color from colorless, to yellow, and finally to orange. After 1 h of reflux, the reaction mixture was removed from heat and cooled in a freezer. A solid precipitate was obtained from cold toluene. The yellow solid was dried overnight in a vacuum oven at 90 °C. Spectroscopically pure product was obtained from the reaction with an overall yield of 90%.

^{1}H NMR (400 MHz, chloroform-d, δ): 8.95 (d, J = 5.7 Hz, 2H), 8.22 (t, J = 2.1 Hz, 2H), 7.45 (dt, J = 5.6, 2.0 Hz, 2H), 4.20–4.06 (m, 8H), 3.33 (s, 2H), 3.27 (s, 2H), 1.33 (td, J = 7.1, 1.7 Hz, 12H).

[Re(4,4′-dimethylphosphonic acid-2,2′-bipyridine)(CO)$_3$Cl] (Catalyst 1). **5** (200 mg, 0.252 mmol) was added to 1 M HCl (5.0 mL) and the mixture was kept at 70 °C for 6 h. Upon cooling to room temperature, the precipitate formed was collected by vacuum filtration and washed with cold methanol and water. Drying first in air and then in vacuum gave **1** as a yellow solid.

^{1}H NMR (400 MHz, acetonitrile-d_3, δ): 8.93–8.80 (m, 2H), 8.41 (s, 2H), 7.52–7.41 (m, 2H), 3.44–3.27 (m, 4H) (Figure S12, SI).

Synthesis of Catalyst 2. Catalyst **2** was synthesized as previously described.[7]

Fabrication of Photoelectrodes and Reference Samples. Thirty nanometers of Cr, followed by 450 nm (nominal) of Au, was deposited on FTO glass (TEC-15, Solaronix, Switzerland) by sputter deposition. The deposition was done using an Alliance Concept DP650 sputtering system (AllianceConcept, France). Cu_2O thin films were deposited onto the gold layer by electrodeposition from a copper lactate solution as described previously[47] for 105 min under a galvanostatic current density of 0.1 mA cm^{-2}. A Pt mesh was used as counter electrode. The copper lactate solution was prepared by dissolving 7.58 g of $CuSO_4$ (Sigma-Aldrich), 67.5 g of lactic acid (Fluka), and 21.77 g of K_2HPO_4 (Sigma-Aldrich) in 250 mL of H_2O. A 2 M KOH solution (Reactolab) was slowly added to the reaction mixture until pH 12 was reached. During this step, the color of the solution changed from dark blue to light blue and finally to dark blue again. Precise adjustment of the pH was achieved using small amounts of KOH and lactic acid.

Atomic layer deposition of the Al:ZnO and TiO_2 layers was carried out on a Savannah 100 system (Cambridge Nanotech) as described previously.[7] Al:ZnO was deposited at 200 °C, whereas the precursors, diethylzinc (ABCR) and trimethylaluminum (ABCR), and H_2O (18 MΩ) were kept at room temperature. Under constant vacuum, the precursor was pulsed for 15 ms, followed by a 10 s wait time. Subsequently, H_2O was pulsed using the same sequence. After 20 cycles of ZnO, 1 cycle of Al_2O_3 was deposited using the same pulse sequence. This was repeated five times, which led to the deposition of 20 nm of Al:ZnO. TiO_2 was deposited under constant vacuum at 150 °C using tetrakis(dimethylamino)titanium (TDMAT; 99%, Sigma-Aldrich) at 75 °C and H_2O_2 (50%, Sigma-Aldrich) at room temperature, using a pulse length of 10 ms, followed by 10 s wait time. In total, 1500 cycles were carried out to yield a TiO_2 film of 100 nm thickness.

After atomic layer deposition of overlayers, the surface of the photoelectrode was subjected to a $TiCl_4$ chemical bath treatment. This was achieved by incubating the samples in 150 mL of 40 mM $TiCl_4$ solution for 30 min at 70 °C. The samples were subsequently rinsed with water and dried in an air stream.

Crystalline mesoporous TiO_2 was deposited onto the surface of the cathodes by screen printing. Commercial 18-NRT TiO_2 paste (Dyesol) was deposited by carrying out two printing steps using a 61T (30.4 cm^3 m^{-2}) screen. The thus-formed films were analyzed by profilometry to exhibit a thickness of 4.5–5 μm.

Curing of the films was carried out at room temperature for 48 h by keeping the film under UV irradiation at 1 mm distance from the lamp (GPH 369T5VA/4 18 W, 253.7 nm peak, Heraeus). Subsequently, the $TiCl_4$ treatment was repeated as described above.

Before catalyst immobilization, water was removed from the mesoporous scaffold by treating the electrode for 30 min at 150 °C under vacuum. Subsequently, the catalyst was immobilized by immersing the electrode for 24 h in a 1 mM solution of catalyst in acetonitrile, followed by copious rinsing with dry acetonitrile.

Reference samples of mesoporous TiO_2 films were prepared directly on FTO glass. UV-treated samples were prepared as follows: FTO glass was pretreated with $TiCl_4$, followed by deposition of the mesoporous scaffold and subsequent treatment steps as described above.

Thermally cured samples were prepared as follows: FTO glass was pretreated with $TiCl_4$, and subsequently, mesoporous TiO_2 was deposited as above. In the next step, the films were cured according to a well-established thermal procedure.[47] $TiCl_4$ post-treatment was carried out as above, followed by heating to 500 °C in a hot air stream

DOI: 10.1021/jacs.5b12157
J. Am. Chem. Soc. 2016, 138, 1938–1946

for 30 min. If catalyst was deposited on the sample, it was immersed in catalyst solution as above while still in a warm state.

Device Characterization. Scanning electron microscopy was carried out using a Zeiss Merlin microscope. FTIR-ATR measurements were carried out using a Spectrum GX system (Perking Elmer), equipped with an ATR extension (MIRacle, Pike Technologies). Each spectrum consists of 50 scans at 4 cm^{-1} resolution. Catalyst loading onto the TiO_2 films were determined as follows: After determination of the surface area, each sample was introduced in a 100 mL Erlenmeyer flask. Subsequently, 2−3 mL of Milli-Q water, 7.5 mL of HCl (Merck 318, Suprapur), and 2.5 mL of HNO_3 (Merck 441, Suprapur) were added. After standing overnight, the mixture was refluxed for 2 h and 20 mL of Milli-Q water was added. The solution was subsequently filtered and the filter washed five times with 2.0 M HNO_3. Subsequently, the volume was completed to 50.0 mL with 2.0 M HNO_3 and the solution analyzed by ICP-OES. Profilometry of TiO_2 films was carried out using an Alpha-Step 500 profilometer. XPS measurements were carried out using a PHI VersaProbe II scanning XPS microprobe.

Electrochemical Testing. Solar simulation was carried out using a LOT Oriel light source, equipped with a 450 W Xe arc lamp (Ozone Free, Osram). The light intensity was reduced by a metal grid, which served as a neutral density filter, followed by a KG3 filter (Edmund Optics). The system was tuned to 1 sun intensity using a calibration diode. Light chopping was carried out using an electromechanical chopper at a frequency of 1 Hz. Samples were tested in a custom-built gastight PEC test cell. The test solution was dry acetonitrile (Sigma-Aldrich) with 0.1 M Bu_4NPF_6 (tetrabutylammonium hexafluorophosphate, Sigma-Aldrich). Electrochemical measurements were performed using a Gamry Interface 1000 and a BioLogic SP-300 potentiostat. A Ag/AgCl wire, separated from the cell by a porous diaphragm, was used as a pseudoreference electrode, and its potential was calibrated to ferrocene. A Pt wire in the same compartment was used as counter electrode. A 3 mm diameter glassy carbon rotating disk electrode (Metrohm) was used for electrochemical characterization of catalysts in solution. In all cases, the solution was saturated either with Ar (Carbagas, 99.9999%) or with CO_2 (Carbagas 99.998%) by sparging the solution with stirring for 20 min. CVs were carried out between −0.4 and −2.4 V vs Fc^+/Fc at 100 mV s^{-1}, whereas linear sweep scans were carried out between the same potentials at 10 mV s^{-1}. Potential-stepping ac-impedance measurements were carried out using a BioLogic SP-300 between 1 MHz and 0.1 Hz.

Gas Measurements. Gas Measurements were carried out under 10 mL min^{-1} flow of CO_2 using the same equipment as described above. Blank tests were carried out, verifying that the counter-electrode in the cell produced negligible CO. Polarization was carried out using the potentiostats described above, and the effluent gas was led into the sampling loop of a gas chromatograph after evaporated acetonitrile was condensed out at −25 °C. The gas chromatograph (Trace ULTRA, Thermo Scientific) was equipped with a ShinCarbon column (Restek) and a PDD detector (Vici). Helium was used as carrier gas.

Catalyst turnover numbers (TON) were calculated by integrating the amount of CO produced during the polarization test and comparing to the measured amount of catalyst.

Spectroelectrochemical Measurements. Spectroelectrochemistry was carried out using the UV−vis equipment and the custom-made test cell described above. An ocean-optics halogen lamp was used to illuminate transparent TiO_2 films on FTO, prepared as described above. A condenser lens behind the film collected the transmitted photons and fed them to an OceanOptics photodiode array by the means of a fiber optic cable. The potential was stepped from −0.4 to −2.4 V vs Fc^+/Fc using a Gamry Framework script. After 20 s equilibration time at each potential, a custom-made LabView software recorded a spectrum from the photodiode array.

■ ASSOCIATED CONTENT

Supporting Information

The Supporting Information is available free of charge on the ACS Publications website at DOI: 10.1021/jacs.5b12157.

Experimental methods, schemes, and supporting results (PDF)

■ AUTHOR INFORMATION

Corresponding Authors

*matthew.mayer@epfl.ch

*michael.graetzel@epfl.ch

Present Address

†Department of Chemistry, University of Zurich, Switzerland.

Notes

The authors declare no competing financial interest.

■ ACKNOWLEDGMENTS

This project was funded by Siemens AG. We would like to express our warmest thanks to T. M. Aufar Kari for the preparation of many samples and for conducting measurements. Further thanks go to Prof. Hubert Girault for helpful discussions, Frédéric Gumy for providing LabView code, to Sylvain Coudret and Karine Vernez Thomas for carrying out ICP-OES analysis, and to Pierre Mettreaux for carrying out XPS measurements.

■ REFERENCES

(1) *Climate Change 2013: The Physical Science Basis - Summary for Policy Makers*; IPCC: Switzerland, 2013.

(2) Lewis, N. S.; Nocera, D. G. *Proc. Natl. Acad. Sci. U. S. A.* **2006**, *103* (43), 15729.

(3) *The Economist* June 13, 2015, http://www.economist.com/news/business/21654082-threaten-fossil-fuels-solar-power-must-solve-its-intermittency-problem-banishing-clouds.

(4) Faunce, T.; Styring, S.; Wasielewski, M. R.; Brudvig, G. W.; Rutherford, A. W.; Messinger, J.; Lee, A. F.; Hill, C. L.; deGroot, H.; Fontecave, M.; MacFarlane, D. R.; Hankamer, B.; Nocera, D. G.; Tiede, D. M.; Dau, H.; Hillier, W.; Wang, L.; Amal, R. *Energy Environ. Sci.* **2013**, *6* (4), 1074.

(5) Luo, J.; Im, J.-H.; Mayer, M. T.; Schreier, M.; Nazeeruddin, M. K.; Park, N.-G.; Tilley, S. D.; Fan, H. J.; Grätzel, M. *Science* **2014**, *345* (6204), 1593.

(6) Kumar, B.; Llorente, M.; Froehlich, J.; Dang, T.; Sathrum, A.; Kubiak, C. P. *Annu. Rev. Phys. Chem.* **2012**, *63* (1), 541.

(7) Schreier, M.; Gao, P.; Mayer, M. T.; Luo, J.; Moehl, T.; Nazeeruddin, M. K.; Tilley, S. D.; Grätzel, M. *Energy Environ. Sci.* **2015**, *8*, 855.

(8) Schreier, M.; Curvat, L.; Giordano, F.; Steier, L.; Abate, A.; Zakeeruddin, S. M.; Luo, J.; Mayer, M. T.; Grätzel, M. *Nat. Commun.* **2015**, *6*, 7326.

(9) Grätzel, M. *Nature* **2001**, *414* (6861), 338.

(10) Bornoz, P.; Abdi, F. F.; Tilley, S. D.; Dam, B.; van de Krol, R.; Graetzel, M.; Sivula, K. *J. Phys. Chem. C* **2014**, *118* (30), 16959.

(11) Brillet, J.; Yum, J.-H.; Cornuz, M.; Hisatomi, T.; Solarska, R.; Augustynski, J.; Graetzel, M.; Sivula, K. *Nat. Photonics* **2012**, *6* (12), 824.

(12) Sato, S.; Arai, T.; Morikawa, T.; Uemura, K.; Suzuki, T. M.; Tanaka, H.; Kajino, T. *J. Am. Chem. Soc.* **2011**, *133* (39), 15240.

(13) Arai, T.; Sato, S.; Kajino, T.; Morikawa, T. *Energy Environ. Sci.* **2013**, *6* (4), 1274.

(14) Arai, T.; Sato, S.; Morikawa, T. *Energy Environ. Sci.* **2015**, *8* (7), 1998.

(15) Dias, P.; Schreier, M.; Tilley, S. D.; Luo, J.; Azevedo, J.; Andrade, L.; Bi, D.; Hagfeldt, A.; Mendes, A.; Grätzel, M.; Mayer, M. T. *Adv. Energy Mater.* **2015**, *5*, n/a DOI: 10.1002/aenm.201501537.

(16) Luo, J.; Li, Z.; Nishiwaki, S.; Schreier, M.; Mayer, M. T.; Cendula, P.; Lee, Y. H.; Fu, K.; Cao, A.; Nazeeruddin, M. K.; Romanyuk, Y. E.; Buecheler, S.; Tilley, S. D.; Wong, L. H.; Tiwari, A. N.; Grätzel, M. *Adv. Energy Mater.* **2015**, *5*, n/a DOI: 10.1002/aenm.201501520.
(17) Dempsey, J. L.; Brunschwig, B. S.; Winkler, J. R.; Gray, H. B. *Acc. Chem. Res.* **2009**, *42* (12), 1995.
(18) Savéant, J.-M. *Chem. Rev.* **2008**, *108* (7), 2348.
(19) Costentin, C.; Robert, M.; Savéant, J.-M. *Chem. Soc. Rev.* **2013**, *42* (6), 2423.
(20) Willkomm, J.; Muresan, N. M.; Reisner, E. *Chem. Sci.* **2015**, *6* (5), 2727.
(21) Costentin, C.; Drouet, S.; Robert, M.; Savéant, J.-M. *Science* **2012**, *338* (6103), 90.
(22) Kumar, B.; Smieja, J. M.; Kubiak, C. P. *J. Phys. Chem. C* **2010**, *114* (33), 14220.
(23) Guerrero, A.; Haro, M.; Bellani, S.; Antognazza, M. R.; Meda, L.; Gimenez, S.; Bisquert, J. *Energy Environ. Sci.* **2014**, *7* (11), 3666.
(24) Costentin, C.; Drouet, S.; Robert, M.; Savéant, J.-M. *J. Am. Chem. Soc.* **2012**, *134* (27), 11235.
(25) Cecchet, F.; Alebbi, M.; Bignozzi, C. A.; Paolucci, F. *Inorg. Chim. Acta* **2006**, *359* (12), 3871.
(26) Windle, C. D.; Pastor, E.; Reynal, A.; Whitwood, A. C.; Vaynzof, Y.; Durrant, J. R.; Perutz, R. N.; Reisner, E. *Chem. - Eur. J.* **2015**, *21* (9), 3746.
(27) Liu, C.; Dubois, K. D.; Louis, M. E.; Vorushilov, A. S.; Li, G. *ACS Catal.* **2013**, *3* (4), 655.
(28) Dubois, K. D.; He, H.; Liu, C.; Vorushilov, A. S.; Li, G. *J. Mol. Catal. A: Chem.* **2012**, *363*−*364*, 208.
(29) Paracchino, A.; Laporte, V.; Sivula, K.; Grätzel, M.; Thimsen, E. *Nat. Mater.* **2011**, *10* (6), 456.
(30) Seger, B.; Pedersen, T.; Laursen, A. B.; Vesborg, P. C. K.; Hansen, O.; Chorkendorff, I. *J. Am. Chem. Soc.* **2013**, *135* (3), 1057.
(31) Seger, B.; Tilley, D. S.; Pedersen, T.; Vesborg, P. C. K.; Hansen, O.; Grätzel, M.; Chorkendorff, I. *RSC Adv.* **2013**, *3* (48), 25902.
(32) Ha, E.-G.; Chang, J.-A.; Byun, S.-M.; Pac, C.; Jang, D.-M.; Park, J.; Kang, S. O. *Chem. Commun.* **2014**, *50* (34), 4462.
(33) Suzuki, T. M.; Tanaka, H.; Morikawa, T.; Iwaki, M.; Sato, S.; Saeki, S.; Inoue, M.; Kajino, T.; Motohiro, T. *Chem. Commun.* **2011**, *47* (30), 8673.
(34) Anfuso, C. L.; Snoeberger, R. C.; Ricks, A. M.; Liu, W.; Xiao, D.; Batista, V. S.; Lian, T. *J. Am. Chem. Soc.* **2011**, *133* (18), 6922.
(35) O'Regan, B.; Grätzel, M. *Nature* **1991**, *353* (6346), 737.
(36) Krawicz, A.; Cedeno, D.; Moore, G. F. *Phys. Chem. Chem. Phys.* **2014**, *16* (30), 15818.
(37) Krawicz, A.; Yang, J.; Anzenberg, E.; Yano, J.; Sharp, I. D.; Moore, G. F. *J. Am. Chem. Soc.* **2013**, *135* (32), 11861.
(38) Seo, J.; Pekarek, R. T.; Rose, M. J. *Chem. Commun.* **2015**, *51* (68), 13264.
(39) Kou, Y.; Nakatani, S.; Sunagawa, G.; Tachikawa, Y.; Masui, D.; Shimada, T.; Takagi, S.; Tryk, D. A.; Nabetani, Y.; Tachibana, H.; Inoue, H. *J. Catal.* **2014**, *310*, 57.
(40) Sahara, G.; Abe, R.; Higashi, M.; Morikawa, T.; Maeda, K.; Ueda, Y.; Ishitani, O. *Chem. Commun.* **2015**, *51* (53), 10722.
(41) Tian, H. *ChemSusChem* **2015**, *8*, 3746.
(42) Arai, T.; Sato, S.; Uemura, K.; Morikawa, T.; Kajino, T.; Motohiro, T. *Chem. Commun.* **2010**, *46* (37), 6944.
(43) Torralba-Peñalver, E.; Luo, Y.; Compain, J.-D.; Chardon-Noblat, S.; Fabre, B. *ACS Catal.* **2015**, *5* (10), 6138.
(44) Dry, M. E. *Catal. Today* **2002**, *71* (3−4), 227.
(45) Smieja, J. M.; Kubiak, C. P. *Inorg. Chem.* **2010**, *49* (20), 9283.
(46) Hawecker, J.; Lehn, J.-M.; Ziessel, R. *J. Chem. Soc., Chem. Commun.* **1984**, 328.
(47) Ito, S.; Murakami, T. N.; Comte, P.; Liska, P.; Grätzel, C.; Nazeeruddin, M. K.; Grätzel, M. *Thin Solid Films* **2008**, *516* (14), 4613.
(48) Paracchino, A.; Mathews, N.; Hisatomi, T.; Stefik, M.; Tilley, S. D.; Grätzel, M. *Energy Environ. Sci.* **2012**, *5* (9), 8673.
(49) Zardetto, V.; Di Giacomo, F.; Garcia-Alonso, D.; Keuning, W.; Creatore, M.; Mazzuca, C.; Reale, A.; Di Carlo, A.; Brown, T. M. *Adv. Energy Mater.* **2013**, *3* (10), 1292.
(50) Arakawa, H.; Yamaguchi, T.; Sutou, T.; Koishi, Y.; Tobe, N.; Matsumoto, D.; Nagai, T. *Curr. Appl. Phys.* **2010**, *10* (2,Supplement), S157.
(51) Blakemore, J. D.; Gupta, A.; Warren, J. J.; Brunschwig, B. S.; Gray, H. B. *J. Am. Chem. Soc.* **2013**, *135*, 18288.
(52) Keith, J. A.; Grice, K. A.; Kubiak, C. P.; Carter, E. A. *J. Am. Chem. Soc.* **2013**, *135* (42), 15823.
(53) Walter, M. G.; Warren, E. L.; McKone, J. R.; Boettcher, S. W.; Mi, Q.; Santori, E. A.; Lewis, N. S. *Chem. Rev.* **2010**, *110* (11), 6446.
(54) Redmond, G.; Fitzmaurice, D. *J. Phys. Chem.* **1993**, *97* (7), 1426.
(55) Takeda, H.; Ohashi, M.; Tani, T.; Ishitani, O.; Inagaki, S. *Inorg. Chem.* **2010**, *49* (10), 4554.
(56) Won, D.-I.; Lee, J.-S.; Ji, J.-M.; Jung, W.-J.; Son, H.-J.; Pac, C.; Kang, S. O. *J. Am. Chem. Soc.* **2015**, *137* (42), 13679.
(57) Fan, K.; Li, F.; Wang, L.; Daniel, Q.; Chen, H.; Gabrielsson, E.; Sun, J.; Sun, L. *ChemSusChem* **2015**, *8* (19), 3242.
(58) Liu, R.; Stephani, C.; Han, J. J.; Tan, K. L.; Wang, D. *Angew. Chem., Int. Ed.* **2013**, *52* (15), 4225.
(59) White, J. L.; Baruch, M. F.; Pander, J. E., III; Hu, Y.; Fortmeyer, I. C.; Park, J. E.; Zhang, T.; Liao, K.; Gu, J.; Yan, Y.; Shaw, T. W.; Abelev, E.; Bocarsly, A. B. *Chem. Rev.* **2015**, *115*, 12888.

DOI: 10.1021/jacs.5b12157
J. Am. Chem. Soc. 2016, 138, 1938−1946